Tampere University

Marco Veltheim

NUCLEAR LOCALIZATION OF DIFFERENT TALIN FORMS AND THEIR INFLUENCE ON GENE EXPRESSION

Faculty of Medicine and Health Technology
Master's Thesis
November 2023

ABSTRACT

Marco Veltheim: Nuclear localization of different talin forms and their influence on gene expression
Master's Thesis
Tampere University
Master's Programme in Biotechnology and Biomedical Engineering
Supervisors: Postdoctoral Researcher Paula Turkki and Professor Vesa Hytönen
Examiners: Postdoctoral Researcher Rolle Rahikainen and University Lecturer Kirsi Rautajoki
November 2023

Talin is an indispensable part of integrin adhesion complexes, protein-based structures that enable a dynamic dialogue between the cell and extracellular matrix in a both biochemical and mechanical manner. This role is closely tied to the mechanosensitive rod domain of talin that mediates information between integrin and the actin cytoskeleton of the cell. The function of talin as an adaptor protein is well-studied and established, but recently talin has been discovered to also localize to the nucleus, where it interacts with chromatin and alters the gene expression profile of the cell.

In this study we wished to find out whether heavily altered forms of talin could also enter the nucleus and influence gene expression. To do so, we introduced increasingly shortened Tln1 variants to cells with their genomic Tln1 eliminated. After this, we evaluated the gene expression profile of the cells by RNA sequencing, as well as observed the subcellular localization of talin forms by confocal microscopy.

It turned out that ectopic talin is treated differently by the cell compared to genomic talin, and shortened talin forms generally cause more downregulation in gene expression compared to full-length wild-type talin. Regarding subcellular localization, all talin forms entered the nucleus, but the form with its entire rod domain removed localized to the nucleus significantly more efficiently than the less altered forms. This might be due to simply the smaller size or because the nuclear localization signal may be in the head domain of the talin molecule. Longer talin forms also probably localize better to the integrin adhesions at the plasma membrane, leaving less molecules to localize to the nucleus.

This study gave a rather general view on the behaviour of altered talin within the cell. In the future, it'd be wise to quantify rRNA in addition to mRNA to find out the possible function of talin inside the nucleoli, as well as study the gene expression profile on the basis of individual genes. The exact location of the nuclear localization signal of talin is also yet to be discovered.

Keywords: Talin, Focal adhesion, Integrin adhesome, Nucleo-adhesome, Subcellular localization

TIIVISTELMÄ

Marco Veltheim: Erilaisten taliinin muotojen tumalokalisaatio ja niiden vaikutus geenieksprессioon
Pro gradu -tutkielma
Tampereen yliopisto
Bioteknologian ja biolääketieteen tekniikan maisteriohjelma
Ohjaajat: tutkijatohtori Paula Turkki ja professori Vesa Hytönen
Tarkastajat: tutkijatohtori Rolle Rahikainen ja yliopistoluennoitsija Kirsi Rautajoki
Marraskuu 2023

Taliini on korvaamaton osa integriiniadheesiokomplekseja, proteiinirakenteita, jotka mahdollistavat dynaamisen vuoropuhelun solun ja soluväliaineen välillä sekä biokemiallisesti että mekaanisesti. Tämä rooli on vahvasti sidoksissa taliinin mekanosensitiiviseen sauvadomeeniin, joka välittää tietoa integriinin ja solun aktiinitukirangan välillä. Taliinin toiminta adapteriproteiinina on hyvin tutkittu ja tieteellisesti perusteltu, mutta viime aikoina taliinin on havaittu lokalisoituvan myös tumaan, jossa se on vuorovaikutuksessa kromatiinin kanssa ja muuttaa solun geenieksprессioprofiilia.

Tässä tutkimuksessa halusimme selvittää, voisivatko voimakkaasti muunnellut taliinin muodot myös siirtyä tuman sisään ja vaikuttaa geenieksprессioon. Tätä varten siirsimme lyhennettyjä Tln1-variantteja soluihin, joiden genominen Tln1 on eliminoitu. Tämän jälkeen arvioimme solujen geenieksprессioprofiilia RNA-sekvensoinnilla ja havainnoimme taliinimuotojen solunsisäistä lokalisaatiota konfokaalimikroskopialla.

Selvisi, että solu kohtelee ektooppista taliinia eri tavalla kuin genomista taliinia, ja lyhennetyt taliinimuodot yleisesti ottaen aiheuttavat enemmän geenieksprессion vaimentumista kuin tehostumista verrattuna täyspitkään villityypin taliiniin. Solunsisäisen lokalisaation kohdalla kaikki taliinimuodot siirtyivät tuman sisään, mutta muoto, josta oli poistettu koko sauvadomeeni siirtyi merkittävästi tehokkaammin tumaan kuin vähemmän muunnellut muodot. Tämä saattaa johtua yksinkertaisesti pienemmästä koosta tai siitä, että tumalokalisaatiosignaali saattaa olla taliinimolekyylin päädomeenissa. Pidemmät taliinimuodot myös luultavasti lokalisoituvat paremmin integriiniadheesioihin, jättäen vähemmän molekyylejä tumalokalisaatioon.

Tämä tutkimus antoi varsin yleisen katsauksen muunnellun taliinin käyttäytymisestä solun sisällä. Tulevaisuudessa olisi viisasta määrittää myös rRNA mRNA:n lisäksi, jotta saataisiin selville taliinin mahdollinen toiminta tumajyvästen sisällä, ja myös tutkia geenieksprессioprofiilia yksittäisten geenien kohdalla. Taliinin tumalokalisaatiosignaalin täsmällinen sijainti on myös yhä selvittämättä.

Avainsanat: Taliini, Fokaaliadheesio, Integriiniadhesomi, Tuma-adhesomi, Solunsisäinen lokalisaatio

PREFACE

I want to thank Postdoctoral Researcher Paula Turkki and Professor Vesa Hytönen for supervising my thesis process, as well as the entire Protein Dynamics research group for providing me with materials, advice and assistance while I conducted the practical work for my thesis. Special thanks to laboratory assistant Niklas Kähkönen for familiarizing me with the laboratory practices and preparing the plasmids used in my work, as well as Latifeh Azizi for helping me on several occasions.

I also want to specifically thank Tampere Imaging Facility (TIF) for allowing me to use one of their microscopes and arranging the training for me, so I was able to operate the device.

Tampere, 8th November 2023

Marco Veltheim

CONTENTS

LIST OF SYMBOLS AND ABBREVIATIONS

ABS	Actin binding site
DEG	Differentially expressed gene
∆	Delta, deletion
DD	Dimerization domain
DKO	Double-knockout
DMEM	Dulbecco's Modified Eagle's Medium
DMSO	Dimethyl sulfoxide
ECM	Extracellular matrix
EGFP	Enhanced green fluorescent protein
F	Talin head (FERM) domain
FA	Focal adhesion
FAK	Focal adhesion kinase
FBS	Fetal bovine serum
FERM	4.1 protein, ezrin, radixin, moesin
FPKM	Expected number of Fragments Per Kilobase of transcript sequence per Millions base pairs sequenced
GO	Gene Ontology
GSEA	Gene Set Enrichment Analysis
IAC	Integrin adhesion complex
IAP	Integrin-associated protein
IBS	Integrin binding site
KANK	Kidney ankyrin repeat-containing protein
KEGG	Kyoto Encyclopedia of Genes and Genomes
KO	Knockout
LIM	Lin11–Isl1–Mec3
MKF	Mouse kidney fibroblast
NMII	Non-muscle myosin II
NLS	Nuclear localization signal/sequence
PFA	Paraformaldehyde
PBS	Phosphate-buffered saline
PIP2	Phosphatidylinositol 4,5-bisphosphate
R	Talin rod domain
RIAM	Rap1-GTP-interacting adaptor molecule
TE-EF	Tris-EDTA, endotoxin-free
TBS	Tris-buffered saline
VBS	Vinculin binding site
WT	Wild-type

1. INTRODUCTION

Talin is a molecule of great interest as it not only serves as a core piece of cell–ECM attachments along with integrin, but also has an effect on gene expression of the cell by itself (Klapholz & Brown, 2017). The true extent of the functions of talin inside the cell has been in focus of recent research.

In this thesis I review the better-known role of talin as a part of integrin adhesion complexes, but the research we conducted delves into the newfound functions related to its localization to the nucleus. Namely we wished to find out how the removal of different structural parts of the talin molecule would affect its localization behaviour and its influence on the gene expression.

Talin is essential for development (Monkley et al., 2000), therefore significant mutations in this protein are presumably embryonic lethal due to severe morphogenetic defects (Azizi et al., 2022), but more subtle alterations cause many diseases, such as cardiovascular malfunction, hematologic disorders and cancer (Da Silva et al., 2022). Thus, understanding the functions of talin at cellular level is crucial in finding potential treatments. For example, it has been discovered that certain somatic mutations in one of the talin isoforms dysregulate cell migration, leading to impaired wound healing when hypoactive (Azizi et al., 2022) or invasive behaviour typical for cancer cells when hyperactive (Azizi et al., 2021). Other mutations disrupt the structural integrity of tissues, causing e.g. spontaneous coronary artery dissection (Turley et al., 2019).

In a wider scope, adhesion proteins localizing to the nucleus have been found to associate with oncogenic behaviour in cells, namely inhibition of apoptosis (Lim et al., 2008) and expression of immunoevasive cytokines (Byron & Frame, 2016). Thus, there is a possibility that targeting these proteins, to which talin also belongs, may be a potential treatment for cancer.

2. LITERATURE REVIEW

Most cells require an extracellular matrix (ECM) for their survival - it provides them signals for i.e. morphogenesis, immune response and healing (Kanchanawong et al., 2010; Klapholz & Brown, 2017). Cells adhere to their surroundings either permanently or dynamically, but most of them are attached to ECM at least during development (Klapholz & Brown, 2017). Integrin is one of the key molecules that anchor the cell into its environment, but it requires a huge amount of other proteins to be functional: these proteins constitute different integrin adhesion complexes (IACs), namely focal adhesions (FAs), focal complexes, fibrillar adhesions, hemiadherens junctions and invadopodia (Klapholz & Brown, 2017). In addition, IACs send signals to the cell in relation to adhesion and mechanical properties of the ECM to regulate its survival, proliferation and differentiation (Gough & Goult, 2018).

In the scope of this thesis, I'll mostly speak of focal adhesions as other IACs have a similar core structure to a relevant degree. The proteins associated to these complexes are the main focus, as they have shown functionality beyond simple adhesion dynamics and thus highlight the importance of talin both as an adaptor and effector molecule.

2.1 Focal adhesions – shaping the cytoskeleton

Focal adhesions are integrin-based cell–ECM attachments (Gough & Goult, 2018). They also play a critical role in force transmission, cytoskeletal regulation and migration (Kanchanawong et al., 2010). The cells come in contact with ECM through trans-plasma-membrane integrins that bind to ECM ligands such as fibronectin, collagen or laminin depending on their specific combination of heterodimeric α and β subunits (Klapholz & Brown, 2017). However, most of the focal adhesion structure consists of an intracellular complex formed from a myriad of cytoplasmic proteins that finally connect the integrins to the actin cytoskeleton (Kanchanawong et al., 2010). These proteins are called integrin-associated proteins (IAPs), among which talin is indispensable (Klapholz & Brown, 2017).

The formation of focal adhesions starts from nascent adhesions located at the leading edge of the lamellipodium (Vicente-Manzanares & Horwitz, 2011). This is an area where active actin polymerization happens, the cytosolic globular actin (G-actin) forming cross-linked filamentous actin (F-actin) that manifests as mesh-like fibres in protrusions of the plasma membrane. The actin in these structures undergoes fast retrograde flow while

the adhesions themselves are relatively immobile (Sun et al., 2016; Vicente-Manzanares & Horwitz, 2011). This adhesion type is very short-lived, but it is also very active in adhesion signalling, recruiting focal adhesion kinase (FAK) to phosphorylate adaptor proteins and thus creating further docking sites for signalling molecules while simultaneously promoting actin polymerization (Vicente-Manzanares & Horwitz, 2011).

The core adaptor protein in the forming adhesion plaque is talin, the head domain of which directly and independently binds both integrin and FAK (Lawson et al., 2012). In turn, FAK phosphorylates and binds an adaptor protein paxillin, initiating a signalling cascade that relays the information about ECM–integrin interaction within the cell (Kanchanawong et al., 2010). Kindlin is an adaptor protein that can both co-operate with talin and also act independently from it by directly binding paxillin and consequently FAK (Theodosiou et al., 2016). This part of the complex is called integrin signalling layer (Kanchanawong et al., 2010). The stratum in the middle of the focal adhesion is force transduction layer that includes talin and vinculin, and finally the innermost is actin regulatory layer with zyxin, α-actinin and vasodilator-stimulated phosphoprotein (VASP). Of these, vinculin, zyxin and VASP can be considered cytoskeletal adaptors while α-actinin acts as a cross-linker between actin filaments. (Kanchanawong et al., 2010). The molecular structure of the described layers can be seen in Figure 1.

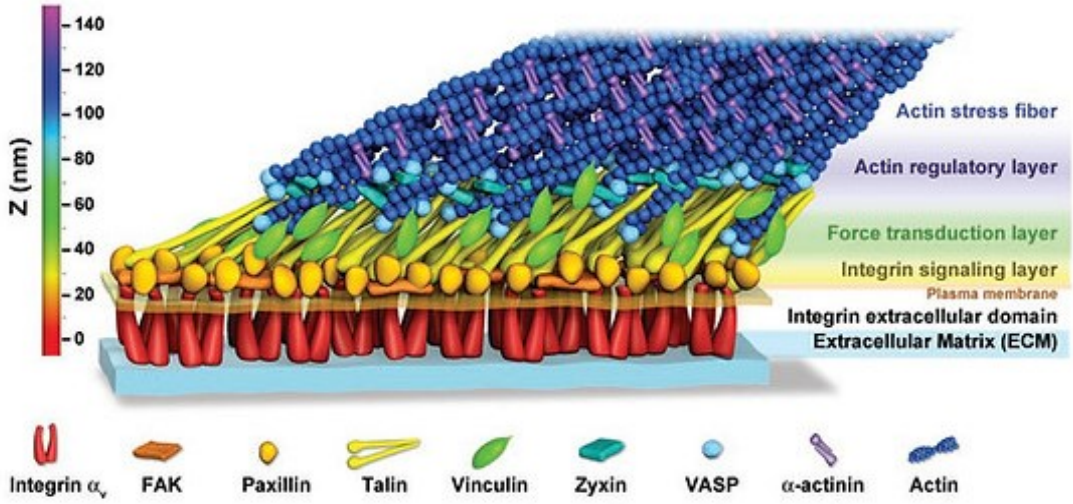

Figure 1. *A schematic model of the molecular architecture within a focal adhesion (Edited from source:* Kanchanawong et al., 2010*).*

The nascent adhesions either disassemble or mature into focal complexes at the rear edge of the lamellipodium as the cell spreads or migrates, their turnover determined by the rate of cell protrusion (Vicente-Manzanares & Horwitz, 2011). The maturation leads to the growth and elongation of the actin filaments into stress fibres and also a decrease in phosphorylation activity by FAK in favour of non-muscle myosin II (NMII) -induced signalling, which is associated with a longer adhesion lifetime (Lawson et al., 2012). Focal complexes exist only transiently, further maturing into bigger and more stable focal adhesions that slow down the retrograde flow of actin filaments and provide the cell with efficient tension-bearing ability and contractibility along with NMII and zyxin (Smith et al., 2014; Vicente-Manzanares & Horwitz, 2011).

Focal adhesions are classified by their size, as bigger protein assemblies correlate with more advanced maturation. Another indicator of this is the replacement of actin-bound NMII-A with NMII-B that leads to more stability and tensile strength as well as slower turnover (Vicente-Manzanares & Horwitz, 2011). Focal adhesions can further mature into large and very stable fibrillar adhesions with prevalent NMII-B signalling that eventually disassemble at the trailing edge of the cell during its retraction (Vicente-Manzanares & Horwitz, 2011). A rough schematic of the arrangement of IAPs in a nascent adhesion, as well as its maturation all the way into a fibrillar adhesion is presented in Figure 2.

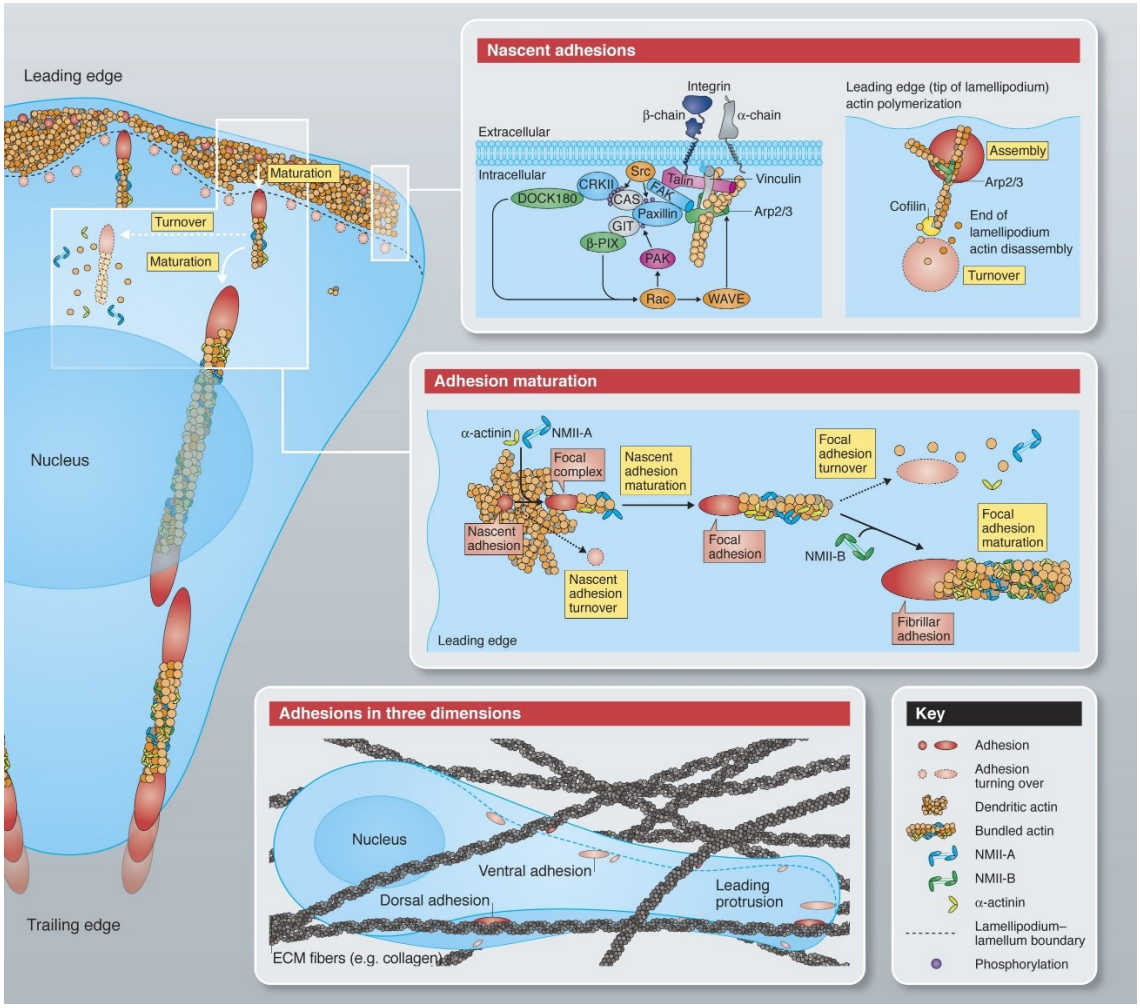

Figure 2. *A schematic of integrin-mediated adhesion dynamics (Edited from source: Vicente-Manzanares & Horwitz, 2011).*

2.2 Talin – the core of focal adhesions

Talin is an interesting protein molecule, as it's actually more conserved among organisms than integrins, indicating that integrins might have evolved after talin, not vice versa (Klapholz & Brown, 2017). Further proof for this theory gives the fact that integrin needs talin for most of its functions, whereas talin has many individual roles, i.e. regulating gene expression (Klapholz & Brown, 2017). All in all, complete absence of talin as well as germline mutations that significantly disrupt its function are embryonic lethal (Azizi et al., 2022).

There are two isoforms of talin in vertebrates: talin-1 and talin-2. They share 88 % similarity and bind the same ligands, alas with different affinities, contributing to fine-tuning of adhesion signalling. They can also act as each other's substitutes in some cases (Gough & Goult, 2018). Still, there are tissue-specific differences in whether talin-1 or talin-2 is the predominantly expressed isoform. For example, talin-2 is more common in

postnatal cardiomyocytes, but in its absence talin-1 has a compensatory effect, rescuing tissue integrity (Manso et al., 2017). Based on scientific evidence so far, talin-1 is the more universal and important isoform, since talin-1 knockout mouse embryos die at gastrulation stage meanwhile talin-2 knockout mice are viable even though they have a somewhat dystrophic phenotype (Gough & Goult, 2018). In this thesis, when I talk about "talin", I'll be referring to talin-1 unless otherwise specified.

Talin has a polarized structure consisting of the N-terminal head, rod domain (R) and the C-terminal dimerization domain (DD) (Gough & Goult, 2018). Figure 3A presents the detailed structure of the talin molecule along with its binding sites that will be discussed in this section.

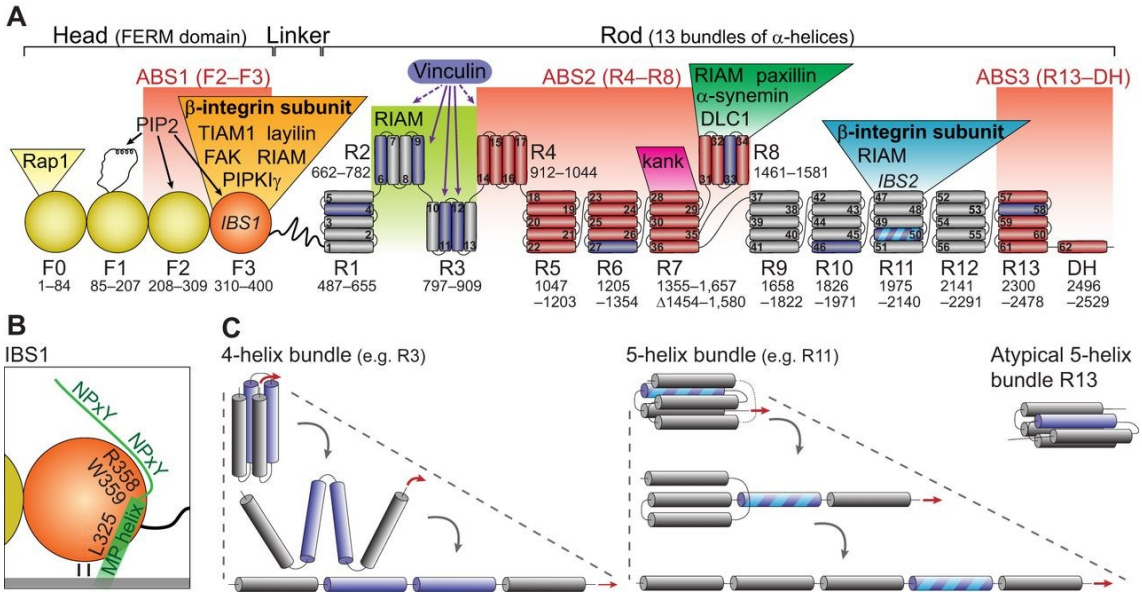

Figure 3. *Structure of the talin molecule and its binding sites (A), interactions of IBS1 (B) and the mechanism of unfolding of the rods (C) (Klapholz & Brown, 2017).*

A specific quality of the talin molecule is that many of its functions are distinct to certain domains or even subdomains and thus can be dissected (Rahikainen et al., 2019). This allows the possibility of using truncated talin forms in studies to pinpoint each function, which is also crucial regarding this thesis.

2.2.1 Talin head domain

The talin head has a so-called atypical 4.1 protein, ezrin, radixin, moesin (FERM) structure, consisting of four subdomains F0 – F3 instead of more common three subdomains F1 – F3 found in several other FERM proteins (Bachmann et al., 2023; Gough & Goult, 2018). FERM domains are often found in proteins that link transmembrane proteins to the cytoskeleton (Klapholz & Brown, 2017). When recruited by the adhesion complex, the talin molecule localizes to the intermediate layer of the adhesion plaque where the head is associated with integrin signalling along with many IAPs such as focal adhesion adaptor proteins paxillin and kindlin, as well as FAK (Kanchanawong et al., 2010). The talin head binds to the cytoplasmic domain of β-integrin (Figure 3B) via its integrin binding site 1 (IBS1) located at the subdomain F3 (Gough & Goult, 2018). Actin binding site 1 (ABS1) is also located at the head domain, specifically at subdomains F2 – F3 (Klapholz & Brown, 2017). The existence and specific order of all the talin head subdomains is considered crucial for sustained integrin activation, and significant mutations in this area are usually embryonic lethal as dysfunctional talin head also impairs the function of integrins (Azizi et al., 2022). However, subtle mutations in some of the subdomains may only slightly alter integrin signalling, leading to a complex disease phenotype (Azizi et al., 2022).

Isolated talin head domain in absence of the entire rod domain (∆R1-R13) can independently act as a signalling molecule through its IBS1 by activating integrins and thus allow the cell to attach to the ECM (Rahikainen et al., 2019). However, it entirely lacks the ability to transduce mechanical forces – a quality associated to the rod domain – rendering the cell incapable of polarization and migration. Also, there are indications that the rod domain is required for increased FAK activation in formation of mature focal adhesions, meaning that FAK responds to both biochemical and mechanical signals (Rahikainen et al., 2019).

2.2.2 Talin rod domain

The rod domain of talin is associated with force transduction along with vinculin and zyxin that work as cytoskeletal adaptors, binding the structure to the actin cytoskeleton at the actin regulatory layer (Kanchanawong et al., 2010). The domain consists of 13 subdomains, R1 – R13, that are formed by α-helix bundles. It also has an integrin binding site, IBS2, that's apparently mainly associated with forming nascent adhesions (Gough & Goult, 2018). More importantly, the rod domain has two actin binding sites, ABS2 formed by R4 – R8 and ABS3 formed by R13 and DD (Klapholz & Brown, 2017), of which C-terminal ABS3 is directly responsible for mechanosensitive unfolding of subdomain R3,

leading to downstream vinculin interaction. On the other hand ABS2 is mainly involved in tension-bearing activity (Gough & Goult, 2018). Vinculin has as many as 11 binding sites (VBSs) at the rod domain, but most of them are only accessible when talin is in a stretched state, making vinculin a stabilizing ligand that strengthens the connection between talin and actin (Gough & Goult, 2018). An exception to this seems to be the VBSs at R8 that are active even in absence of mechanical load and thus contribute to the formation of nascent adhesions (Han et al., 2021). Additionally, the kidney ankyrin repeat-containing (KANK) protein binding site at R7 is associated with microtubule recruitment to the adhesion sites. The binding of KANK family proteins also negatively regulates the attachment of actin to the nearby ABS2 (Sun et al., 2016).

Talin molecule with its rod subdomains 1 – 12 removed (∆R1-R12) is capable of activating integrins, but it can also partake in inducing adhesion stability thanks to ABS3 at R13 (Rahikainen et al., 2019). However, it still lacks all the mechanoregulated rod subdomains that are able to bind vinculin, so adhesion reinforcement and migration are dysfunctional. This makes sense as lamellipodial tension seems to be a key factor in enabling these processes (Schulte et al., 2016). On the other hand, both ∆R1-R10 talin with two VBSs and ∆R4-R12 talin with six VBSs independently enable these functions, indicating that either rod subdomains 1 – 3 or 10 – 12 are needed for sufficient functionality that leads to cell polarization (Rahikainen et al., 2019).

2.2.3 Talin dimerization domain and autoinhibition

As the name suggests, the dimerization domain can bind another talin molecule, forming homodimeric talin (Gough & Goult, 2018). This structure is capable of autoinhibition, forming a “double donut” with the head domains hidden inside, making it unable to bind integrins (Klapholz & Brown, 2017). Specifically, F3 subdomain of the head binds the R9 subdomain of the rod, creating the most important autoinhibitory fold, though also other similar interactions between head and rod have been proposed (Bachmann et al., 2023). This conformation remains inactive in the cytosol until it receives an activation signal. This kind of inactivation of talin is important, because too high level of integrin activation is shown to be detrimental for morphogenesis (Klapholz & Brown, 2017). Known activators for talin include phosphatidylinositol 4,5-bisphosphate (PIP2), which is especially important as a plasma membrane protein in organisms lacking integrin, as well as Rap1-GTPase and its interacting adaptor molecule (RIAM). Rap1 and RIAM are key factors in advancing the activation of talin to the activation of integrin (Bachmann et al., 2023; Klapholz & Brown, 2017).

2.3 Integrin activation – all routes cross at talin

Conformational changes in integrin increase or decrease its affinity for ECM ligands, leading to its activation or deactivation. The states they go through spontaneously involve two closed conformations, inactive bent form and low-affinity extended form (Klapholz & Brown, 2017). The high-affinity open conformation is only attainable by interacting with talin and apparently also with kindlin (Theodosiou et al., 2016). There are two ways of integrin activation: inside-out activation mediated by active binding of talin to the intracellular side of integrin, and outside-in activation, mediated by passive binding of ECM ligands to the extracellular side of it (Klapholz & Brown, 2017). Specifically, in the first case talin activation leads to integrin activation, and in the second case integrin activation leads to talin activation (Bachmann et al., 2023). Figure 4 presents two different routes of interaction between ECM, integrin, talin and finally actin that lead to integrin activation (Figure 4A-D). Eventually this can induce mechanotransduction (Figure 4E). The first route includes utilization of IBS2 along with IBS1 while the second only uses IBS1 at the heads of the dimer.

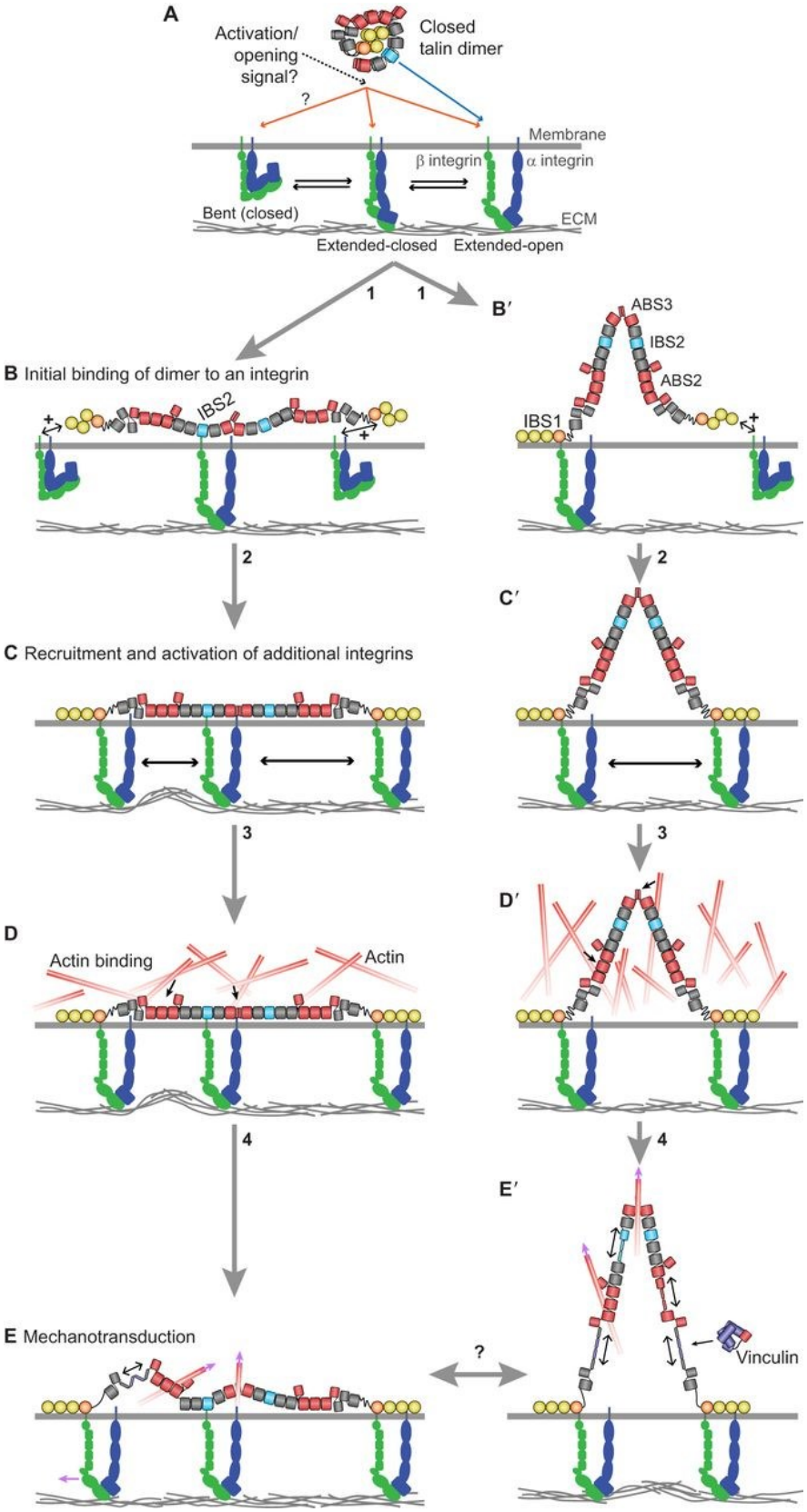

Figure 4. *Assembly of the ECM–integrin–talin–actin link. Panel A shows the inactive state of talin and the three activation states of integrin. Panels B-E show two alternative routes of interaction between integrin, talin and actin (Klapholz & Brown, 2017).*

The inside-out activation of integrins is induced by the binding of talin to the α and β subunits of integrin heterodimer (Klapholz & Brown, 2017). This is initiated by an activation signal, specifically in a Rap1-GTPase-dependent pathway where Rap1 binds to the F0 subdomain of talin, dissociating the F3 – R9 interface of the autoinhibited talin dimer that hides the binding sites for integrin (IBS1), PIP2 and paxillin located in the head domain, as well as the C-terminal ABS3 (Figure 3A)(Bachmann et al., 2023; Gough & Goult, 2018). The activation cascade goes on as Rap1 also interacts with RIAM, exposing its talin binding site that allows it to associate with multiple subdomains of talin (Figure 3A). Finally, Rap1 and RIAM aid in bringing talin to interact with plasma membrane-bound PIP2 (Bachmann et al., 2023). Consequently, as the released IBS1 in F3 subdomain of talin binds the cytoplasmic tail of β-integrin, the orientation of the transmembrane domain of the entire heterodimer changes, separating the α and β subunits from each other (Figure 4B), thus inducing a high-affinity open conformation of integrin (Klapholz & Brown, 2017). This activation route is crucial in hematopoietic cells as they often need to catch sparse and moving ligands, as well as in mesenchymal cells that utilize dynamic focal adhesions for migration (Klapholz & Brown, 2017; Theodosiou et al., 2016).

The outside-in activation of integrins happens usually when the cell is in a constant contact with ECM such as epithelial cells sitting on basal membrane or when the concentration of ECM ligands is high in general (Bachmann et al., 2023; Klapholz & Brown, 2017). Unbound integrins are in equilibrium of bent and extended states (Figure 4A), and when a ligand is available, the extended conformation spontaneously binds it (Klapholz & Brown, 2017). This triggers the integrin activation cascade, recruiting talin to the adhesion complex in a Rap1-independent manner. Mn^{2+}-induced integrin clustering proves that integrin can interact with talin head even in absence of other IAPs (Bachmann et al., 2023). In turn this can also lead to inside-out activation as bound talin can use its IBS2 to bind an adjacent integrin (Figure 4B-C), activating it as well. As a homodimer, full-length talin is capable of binding a total of four integrins (Klapholz & Brown, 2017). The binding of talin head to integrin also increases integrin clustering at the plasma membrane independently from other activators (Bachmann et al., 2023).

2.4 Mechanotransduction – communication through talin

The ability of talin to transduce force is closely tied to its rod domain that is capable of unwinding when it’s stretched by actomyosin pulling and reverting back to its original form in rest (Figure 3C). While stretching, cryptic vinculin binding sites are revealed (Figure 4E’), allowing protein-specific stratification of vinculin and actin (del Rio et al., 2009; Hytönen & Vogel, 2008; Kanchanawong et al., 2010). Binding of vinculin also seems to

alleviate repression of other binding sites such as ABS2, facilitating the binding of actin to the rod domain (Klapholz & Brown, 2017). Higher tension within the talin molecule clearly correlates with higher actin arrangement both at ABSs and vinculin (Kumar et al., 2018). These characteristics make talin a molecular mechanosensor (Elosegui-Artola et al., 2018). On the other hand, the unwound talin is incapable of binding RIAM and KANK as their binding sites become abolished, showing how talin has a switch-like functionality (Gough & Goult, 2018).

With this control over actin alignment, talin and vinculin form the so-called “molecular clutch”, relaying spatial information from cytoskeleton to plasma membrane by pulling on the cytoplasmic tails of integrins and thus directing its activation state (Elosegui-Artola et al., 2018; Gough & Goult, 2018; Kanchanawong et al., 2010). In the other direction, information about integrin activation is relayed to the cytoskeleton, causing actin assembly in upregulated and disassembly in downregulated state (Park et al., 2020). Basically, dense ECM requires more adhesions just for the cell to attach on or move between the meshwork of fibres, so outside-in activation is utilized a lot, leading to increase in actin bundling. This, in turn, allows the cell to withstand more mechanical strain (DeWane et al., 2021).

Mechanotransduction is fully impaired in the absence of the talin rod domain, but mere presence of R13 enables significant anisotropic spreading and stable cell adhesion, indicating the key role of R13 in initiating the mechanical activation of the rest of the rod domain (Rahikainen et al., 2019). However, ∆R1-R12 talin lacks the dynamic adaptability of the talin forms with additional subdomains, making the adhesions rigid and fragile, while adhesions with ∆R1-R10 or ∆R4-R12 talin can resist actomyosin contraction and support controlled assembly and disassembly of the cell–ECM attachments required for migration (Rahikainen et al., 2019).

Finally, mechanotransduction has an effect on many significant cellular processes by either causing instant structural changes or by initiating biochemical signalling pathways (Smith et al., 2014). This can be seen directly as substrate sensing and patterns of cell migration and indirectly as transcription regulation (Rahikainen et al., 2019). Through altered gene expression, the cell can remodel the ECM according to its needs or differentiate its own phenotype to suit it (Schwartz, 2010). The composition of the ECM can even affect the metabolic rate of the cell as it has to adapt to the stiffness of its microenvironment (DeWane et al., 2021). Overall, dynamic dialogue between cell and ECM is a necessary part of tissue homeostasis (Kumar et al., 2018; Smith et al., 2014).

2.5 Adhesomes – adhesion proteins in various locations

Integrin adhesome is a term used for a group of proteins that participate in the formation of integrin adhesion complexes (Klapholz & Brown, 2017). Beside this group, talin – specifically the isoform talin-1 – has also been found to belong to nucleo-adhesome that consists of adhesion proteins localizing to the nucleus (Byron et al., 2022). The reason for this phenomenon has been unclear, but it seems related to transcription regulation during cellular stress such as oncogenesis (Byron & Frame, 2016). It has recently been perceived that talin-1 interacts with chromatin and its deletion drastically changes gene expression profile (Da Silva et al., 2022).

The most well-studied member of the nucleo-adhesome is FAK that not only localizes to the integrin adhesion complexes, but to the nucleus as well (Byron et al., 2022). This is indicative of an additional signalling function of the protein besides being a component of the adhesion plaque. Inside the nucleus FAK works along with nuclear protein Hic-5 as a transcription regulator of genes coding other adhesion proteins (Byron et al., 2022). Additionally, during oncogenesis FAK accumulates into the nucleus to regulate the expression of immunoevasive cytokines (Byron et al., 2022; Byron & Frame, 2016). FAK also inhibits apoptosis by deactivating tumour suppressor gene p53 (Lim et al., 2008).

Some other nucleo-adhesome proteins include zyxin, paxillin, α-actinin, kindlin-2 and talin-1 that most likely also have a role in transcription regulation (Byron et al., 2022). One common structure for these is the LIM (Lin11–Isl1–Mec3) domain in zyxin and paxillin which is known to enable proteins to translocate between nucleus and cytoplasm and affect both cytoskeletal dynamics and gene expression (Kadrmas & Beckerle, 2004; Smith et al., 2014). Another possible domain of interest that is shared between FAK, kindlin and talin is the FERM domain that has been hypothesized to contain a nuclear localization signal (NLS) (Byron et al., 2022). In the case of FAK, making the FERM domain inaccessible effectively prevents its nuclear translocation (Brami-Cherrier et al., 2014).

3. OBJECTIVES

Our goal was to express talin truncations in cells and observe their behaviour regarding alterations in their gene expression profile and subcellular localization of the truncated talin.

In a pre-print by Da Silva et al. (2022) it was perceived that absence of talin-1 greatly alters gene expression in human breast epithelial cells, upregulating 318 genes while downregulating 419 of them. Consequently, we wished to see how mouse kidney fibroblast cells with both Tln1 and Tln2 genes eliminated and transfected with various Tln1 forms express their genes compared to cells with wild-type talin. Simultaneously we were keen to evaluate whether the talin forms enter the nucleus and in what degree they do so. From previous research it seems that talin-1 localizes to the nucleus and is even considered part of the nucleo-adhesome (Byron et al., 2022). It also seems that talin-1 interacts strongly with chromatin in human breast epithelial cells (Da Silva et al., 2022). We wished to find out if this holds true for the truncated talin forms as well.

The talin forms we chose for the study were ∆R1-R13 (talin head) and ∆R1-R12 as they can be considered the simplest functional forms of talin – head enables integrin signalling while ∆R1-R12 additionally enables rudimentary focal adhesion dynamics. Full-length wild-type talin was included as a reference. With this, we can pinpoint how the structural differences affect gene expression and subcellular localization of talin.

4. MATERIALS AND METHODS

4.1 Cells and culturing

The cell line used for the study was Tln1$^{-/-}$Tln2$^{-/-}$ (talin double-knockout/DKO) mouse kidney fibroblasts (MKF) described by Theodosiou et al. (2016), thawed from liquid nitrogen storage in 10% dimethyl sulfoxide (DMSO). Tln2$^{-/-}$ (talin-2 knockout/2KO) cells from the parental cell line were used as positive control and reference. The cells were maintained in 1 x Dulbecco's Modified Eagle's Medium (DMEM) + GlutaMAX™ [+] 4.5 g/l D-Glucose [-] Pyruvate (Gibco) with 10% fetal bovine serum (FBS), seeded on BioLite Flask (Thermo Fisher Scientific) in 5% CO_2 and 37 ℃ incubator.

Throughout the maintenance the cells were observed under Zeiss Axio phase contrast microscope and split by washing with 1 x phosphate-buffered saline (PBS), detaching with TrypLE™ Express [-] Phenol Red (Gibco) and redistributing a fraction of the cells into a new flask as the confluence of the culture neared 100%.

Before further processing, a 10 µl sample of the cell suspension was counted, diluted 1:1 in Trypan Blue Stain 0.4% (Invitrogen) to evaluate the viability of the culture.

4.2 Transfection

The Tln1 variants were introduced to the cells subcloned into pEGFP-C1 plasmid backbone (Clontech). The plasmid has a gene expressing enhanced green fluorescent protein (EGFP) attached to the 3' end of the inserted gene, working as a tag for visual recognition (protein of interest expressed with C-terminal EGFP fusion protein). The genes were inserted as cDNA of following constructs: full-length wild-type (WT) Tln1, Tln1 ∆R1-R12 (head + R13 + DD) and Tln1 ∆R1-R13 (talin head), characterized by Rahikainen et al. (2019). Figure 5 presents the schematics of the proteins expressed by these genes.

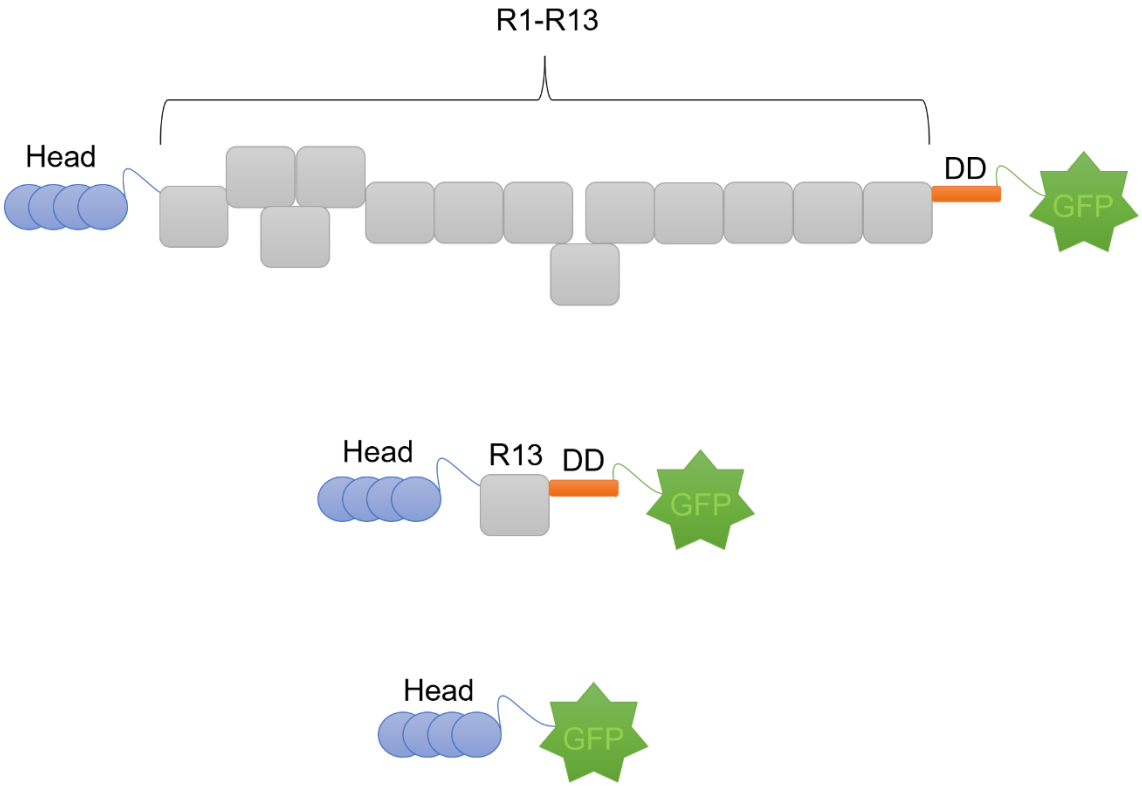

Figure 5. *Schematics of the used talin variants: full-length wild-type, ΔR1-R12 and head.*

Through optimization, 6 x 10^6 cells per transfection was found to be a sufficient for use simultaneously for RNA isolation and SDS-PAGE analysis. For confocal imaging, 1 x 10^6 cells per transfection were used.

The required mass of wild-type Tln1 plasmids was considered to be about 6 µg per 1 x 10^6 cells. For 6 x 10^6 cells used in RNA isolation and SDS-PAGE it was rounded up to 30 µg. As this was for a 12 357 bp plasmid, the mass of 6902 bp Tln1 ΔR1-R12 and 6177 bp Tln1 head needed to be adjusted according to their size so that roughly equal numbers of plasmids would be transferred into the cells. Thus, the mass of Tln1 ΔR1-R12 plasmids ended up being 16.76 µg and Tln1 head 15 µg. For confocal imaging the corresponding values were 6 µg of WT Tln1, 3.35 µg of Tln1 ΔR1-R12 and 3 µg Tln1 head. When preparing the samples, 20% extra was included to compensate for loss of materials during processing.

The plasmids were used as solutions in endotoxin-free Tris-EDTA (TE-EF) buffer, so the final volumes were calculated from their concentrations.

As preparation for transfection, the required volume of cell suspension was calculated based on the obtained cell count. The media was removed from it by centrifuging at 150 g for 5 min at RT and removing the supernatant. The cells were washed with 1 x PBS

that was removed in the same way. The pellet was resuspended in Neon™ Resuspension Buffer R (Invitrogen). 120 µl of the suspension was mixed with the required volume of each plasmid solution. Negative control was left without the plasmids, but otherwise processed the same way.

The cells were transfected with Neon™ Transfection System (Thermo Fisher Scientific) by 1350 V, 30 ms, one-pulse electroporation within a device-specific pipette submerged into Electrolytic Buffer E2 (Invitrogen), after which the cells were instantly moved into 1 ml of media.

4.3 RNA isolation

The transfected cells and controls were seeded on BioLite 60 mm Tissue Culture Dish (Thermo Fisher Scientific) that had been coated with 2 ml of 10 µg/ml human fibronectin in 1 x PBS to provide the cells with a defined and homogenous surface for growth and additionally prevent non-transfected cells from attaching. Before seeding, the fibronectin had been allowed to attach for about three hours at 37 °C, after which the excess solution was removed and replaced with 2.5 ml of media. Save for the positive control (2KO cells), the cells were seeded on the dishes in the volume of 800 µl.

The positive control didn't go through electroporation at all, instead 2.5 x 10^6 cells were seeded on the dishes as-is.

Within 24 hours from transfection and/or seeding the overall gene expression of the cells was studied by isolating their RNA with RNeasy® Mini Kit (Qiagen) according to following protocol:

The media was removed from the dish, after which transfected cells were washed with 2 ml of 1 x PBS to facilitate the removal of non-transfected cells. Controls weren't washed.

The cells were disrupted by addition of 600 µl of Buffer RLT that had 10 µl β-mercaptoethanol per 1 ml of buffer added to it to inhibit RNAses. The lysate was collected and then homogenized by passing it through a 21 G needle ten times. 600 µl of 70% ethanol was added and the lysate was mixed.

The kit protocol was followed until the Buffer RPE wash that was performed three times. Additionally, the third dose of Buffer RPE was left in the spin column for 5 minutes before centrifugation to ensure the best possible removal of guanidine residue.

For RNA elution, 40 µl of RNAse-free water was added to the spin column before centrifugation. As the RNA yield was expected to be low, the eluate was centrifuged through the spin column a second time.

30 µl of the eluate was immediately stored at -20 ℃, while 10 µl was used to determine its concentration and purity with NanoDrop One (Thermo Fisher Scientific). All samples were analysed three times.

The entire process of transfection and RNA isolation was repeated until three samples of each talin variant culture and control with following values were obtained as required by Novogene: total RNA ≥ 200 ng/µl, A260/A280 = 1.8 – 2.2 and A260/A230 ≥ 1.8. After this, the samples were sent for further analysis to Novogene.

4.4 SDS-PAGE and Western blot

Along with RNA isolation, a portion of the cells was prepared for SDS-PAGE in order to study the expression level of proteins.

The positive control was seeded on the 60 mm culture dishes as with RNA isolation, meanwhile the electroporated cells were seeded in the volume of 200 µl on BioLite 6 Well Multidish (Thermo Fisher Scientific) plates. Also, the plates were coated with 10 µg/ml fibronectin in 1 x PBS, in the volume of 1 ml per well, later replaced with 1.5 ml of media.

Within 24 hours from transfection and/or seeding the samples were prepared for SDS-PAGE by first removing the media and thereafter washing the transfected cells with 1 ml of 1 x PBS. Controls weren't washed. The positive control was lysed by addition of 120 µl of 2 x laemmli buffer + 1:20 β-mercaptoethanol, while other cultures required only 80 µl of it. The resulting lysate was collected and stored at -20 ℃

The prepared samples were boiled in a 100 ℃ heat block for 5 minutes, after which they were spinned to return the liquid condensed on the lid of the tube back into the sample. As the size of the extracted proteins was assumed to be around 50 – 270 kDa, the gel chosen for the SDS-PAGE was Criterion™ TGX Stain-Free™ Precast Gels Any kD™ 26 well comb 15 µl/1.0 mm (Bio-Rad). The gel was submerged in 1 x SDS-PAGE Running Buffer consisting of 25 mM Tris, 190 mM glycine and 0.1% SDS. The ladder used was Precision Plus Protein All Blue Standards (Bio-Rad), diluted 1:10 in 1 x PBS.

The electrophoresis was done with Bio-Rad Powerpac Basic device with constant current. The values for the run were 60 A for 15 minutes and 80 A for 25 minutes. The gel was thereafter processed with Trans-Blot Turbo™ Transfer System (Bio-Rad), using

Trans-Blot Turbo™ Transfer Pack, Midi Format, 0.2 µM Nitrocellulose, single application (Bio-Rad). The program used was High MW for Midi-size gel, 2.5 A / 25 V / 10 min.

The extracted nitrocellulose was incubated in Every Blot Blocking Buffer (Bio-Rad) at RT for 5 minutes on a shaker, after which following primary antibodies were added diluted into the blocking buffer: Goat Anti-GFP (#AB0020-500, Sicgen) in ratio of 1:1000 and Mouse Anti-actin Clone C4 (#MAB150IR, Millipore) in ratio of 1:2000. The nitrocellulose was incubated in the primary antibody solution at + 4 ℃ overnight on a shaker.

The primary antibodies were removed, and the nitrocellulose membrane was washed with 0.05% Tris-buffered saline (TBS) -Tween for 5 minutes, three times total. The secondary antibody Horse Anti-Mouse IgG (H+L) peroxidase (#PI-2000, Vector Laboratories) was added diluted 1:20 000 into 1 x TBS to detect actin. The membrane was incubated at RT for 1 hour, after which it was washed as previously, and processed with WesternBright™ ECL Western blotting detection kit Chemiluminescent HRP substrate (Advansta) according to the protocol. The ladder was also drawn on the membrane with WesternSure Pen (LiCOR). The membrane was scanned with Bio-Rad Chemidoc reader with five second illumination.

The secondary antibody Peroxidase labeled Anti-Goat IgG (H+L) affinity purified made in Horse (#PI-9500, Vector Laboratories) was added diluted in 1:20 000 into 1 x TBS to detect GFP. The membrane was incubated at + 4 ℃ overnight on a shaker, after which it was processed similarly as with the actin antibody. The intensities of the resulting bands were measured with ImageJ (Fiji).

4.5 Confocal imaging

The transfected cells and negative control were seeded on coverslips placed on BioLite 12 Well Multidish (Thermo Fisher Scientific) that had been coated with 1 ml of 10 µg/ml fibronectin in 1 x PBS and later replaced with 1 ml of media. From every transfected cell line (full-length WT Tln1, Tln1 ∆R1-R12 and Tln1 head), as well as negative control, 150 µl of cell suspension was seeded on five wells. The process was repeated three times to produce triplicate samples.

Within 24 hours from electroporation, the media was removed, and the wells were washed with 1 ml of 1 x PBS. The cells were fixed by adding 500 µl of 4% paraformaldehyde (PFA) in 1 x PBS per well and incubating for 20 minutes at RT, after which PFA was removed, and the wells were filled with 1 x PBS for storage at + 4 ℃. The entire fixing process, storage and all following procedures were conducted in a dark room.

For mounting, PBS was removed and replaced with 1 ml of Milli-Q water to get rid of salts. The coverslips were placed on objective glass with Prolong™ Diamond Antifade Mountant with DAPI (Invitrogen). For each talin variant and negative control, two coverslips were mounted.

The imaging was conducted with Zeiss LSM800 confocal microscope. The images were taken from 5 representative cells on each coverslip with 63 x magnification using channels 488 nm (GFP) and 405 nm (DAPI) and 0.24 µm Z-stack slices. The following data analysis was done with ImageJ (Fiji) by measuring the raw integrated densities of GFP signal (488 nm) inside the nucleus and the whole cell from 4 focal planes (Z-stack slices) around the centre of the nucleus as roughly indicated in Figure 6, described in more detail in the next section. Statistical analysis was conducted with IBM SPSS Statistics 26, using one-way ANOVA with Bonferroni test to determine statistical significance.

Finally, WoLF PSORT protein localization predictor (https://wolfpsort.hgc.jp/) was used to evaluate the possible location of the nuclear localization signal.

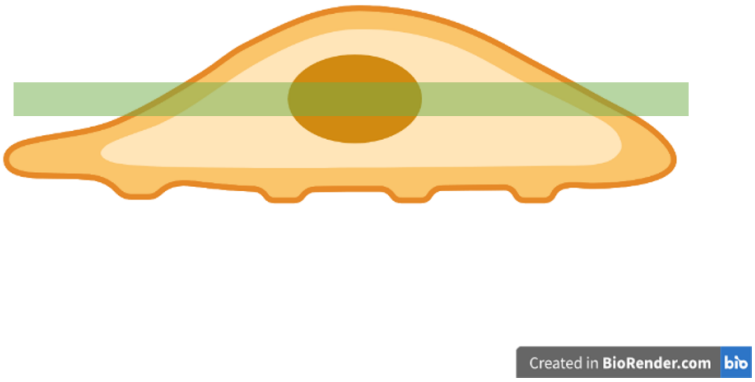

Figure 6. *Schematic of the area where the raw integrated densities of GFP signal were calculated. The green bar represents the chosen 4 focal planes used in analysis.*

5. RESULTS

5.1 Optimization of RNA isolation

Before deciding the exact method of RNA isolation, the protocol was optimized as indicated in Table 1, where values for full-length WT Tln1 are shown as reference. The same protocol was utilized for other constructs and negative control. The positive control didn't go through electroporation, and its proliferation rate was observed to be much higher, so 2.5 x 10^6 cells were deemed sufficient.

Table 1. *Optimization of the RNA isolation protocol.*

Setup	Problem	Corrective measures	Outcome
2x10^6 cells /transfection 700 µl Buffer RLT 18 G needle 2x wash with Buffer RPE 30 µl water for elution	Low yield (~95 ng/µl) Low A260/A230 (~0.17)	Number of cells increased to 5x10^6 cells /transfection	Better yield (~330 ng/µl) Better A260/A230 (~0.89)
5x10^6 cells /transfection 700 µl Buffer RLT 18 G needle 2x wash with Buffer RPE 30 µl water for elution	Low A260/A230 (~0.89)	Amount of Buffer RLT decreased to 350 µl	Lower yield (~130 ng/µl) Lower A260/A230 (~0.70)
5x10^6 cells /transfection 350 µl Buffer RLT 18 G needle 2x wash with Buffer RPE 30 µl water for elution	Low yield (~130 ng/µl) Low A260/A230 (~0.70)	Needle gauge size increased to 21 G Amount of water increased to 40 µl + 1 wash with Buffer RPE (5 min incubation after the 2nd)	Better yield (~340 ng/µl) Better A260/A230 (~1.7)
5x10^6 cells /transfection 700 µl Buffer RLT 21 G needle 3x wash with Buffer RPE 40 µl water for elution	Low A260/A230 (~1.7)	Amount of Buffer RLT decreased to 600 µl Number of cells increased to 6x10^6 cells /transfection	Better yield (~380 ng/µl) Better A260/A230 (~2.2)
6x10^6 cells /transfection 600 µl Buffer RLT 21 G needle 3x wash with Buffer RPE 40 µl water for elution	None	None	All values satisfactory (total RNA ≥ 200 ng/µl, A260/A280 = 1.8 – 2.2, A260/A230 ≥ 1.8)

The mRNA purified from total RNA went through RNA sequencing, gene count and finally differential gene expression analysis, all conducted by Novogene. In the next subsection I briefly describe the analysis based on the received documentation.

5.2 RNA sequencing

To construct a library of reads the purified mRNA was fragmented, reverse transcribed into cDNA and amplified by RT-qPCR, after which the reads were cleaned and aligned to the reference genome with Hisat2 v2.0.5. These mapped reads were assembled in StringTie v1.3.3b, and the number of reads mapped to each gene was counted with FeatureCounts v1.5.0-p3. FPKM (expected number of Fragments Per Kilobase of transcript sequence per Millions base pairs sequenced) was calculated for each gene based on gene length and the reads count to take into consideration both the effect of sequencing depth and the length of the gene.

After the gene expression level was quantified, differential expression analysis of two groups with two biological replicates per group was conducted with DESeq2R package 1.20.0. Benjamini and Hochberg's method was used to adjust the obtained P-values in order to control the false discovery rate. Genes found by DESeq2 with an adjusted P-value ≤ 0.05 were assigned as differentially expressed genes (DEGs).

To correct the gene length bias, Gene Ontology (GO) enrichment analysis of differentially expressed genes was performed using clusterProfiler R package. GO terms with corrected P-value < 0.05 were considered significantly enriched. Similar enrichment analysis was done with Kyoto Encyclopedia of Genes and Genomes (KEGG) pathways. Finally, Gene Set Enrichment Analysis (GSEA) was utilized to determine if a pre-defined gene set can show a significant consistent difference between two biological replicates. The used data sets were from GO and KEGG.

The differential expression levels can be seen in Figure 7, where each set of bars corresponds to a comparison between two groups of samples. Down- and upregulated gene counts are presented, as well as the sum of both.

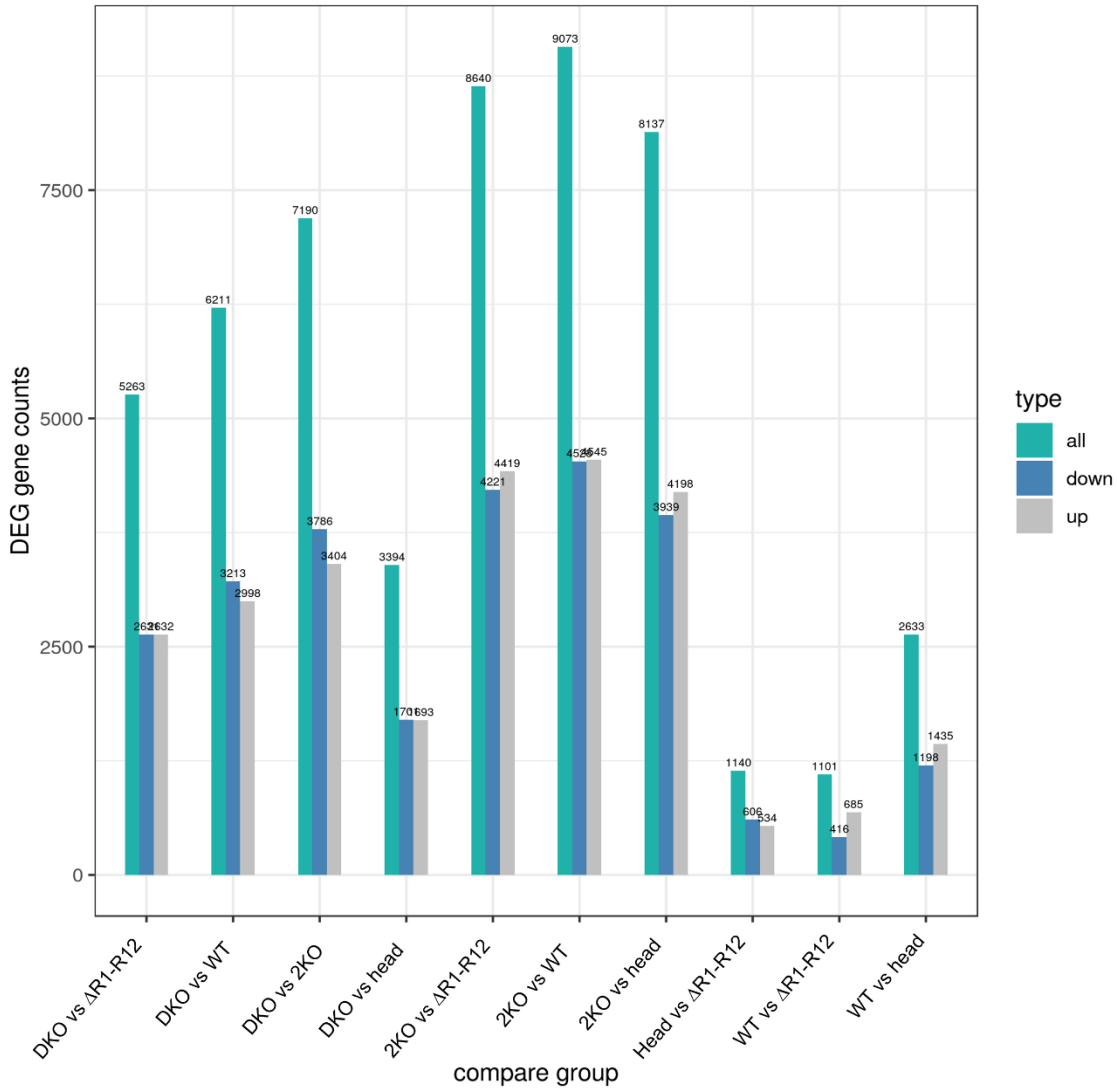

Figure 7. *Differential gene expression. Graph of the results of RNA-Seq gene count and differential expression analysis of two groups (two biological replicates per group), performed by Novogene. Genes with an adjusted P-value ≤ 0.05 found by DESeq2 were assigned as differentially expressed genes (DEGs).*

5.3 SDS-PAGE and Western blot to evaluate talin expression

Protein quantification was done to ensure that all constructs were being expressed. First, to evaluate the number of cells in each sample, immunostaining for actin was performed (Figure 8). The final obtained Western blot image after immunostaining also for GFP is presented in Figure 9.

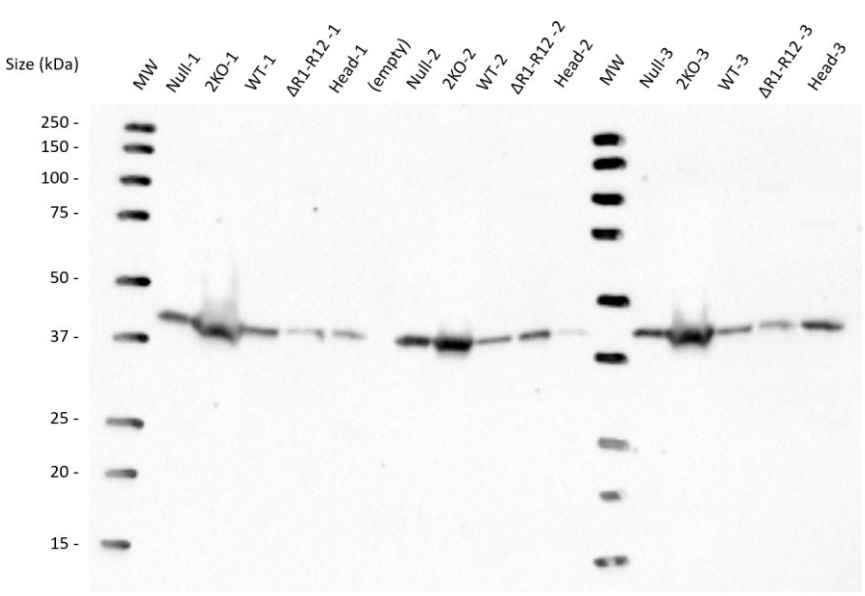

Figure 8. *Western blot image for actin, stained with Mouse Anti-actin Clone C4 (#MAB150IR, Millipore) and Horse Anti-Mouse IgG (H+L) peroxidase (#PI-2000, Vector Laboratories).*

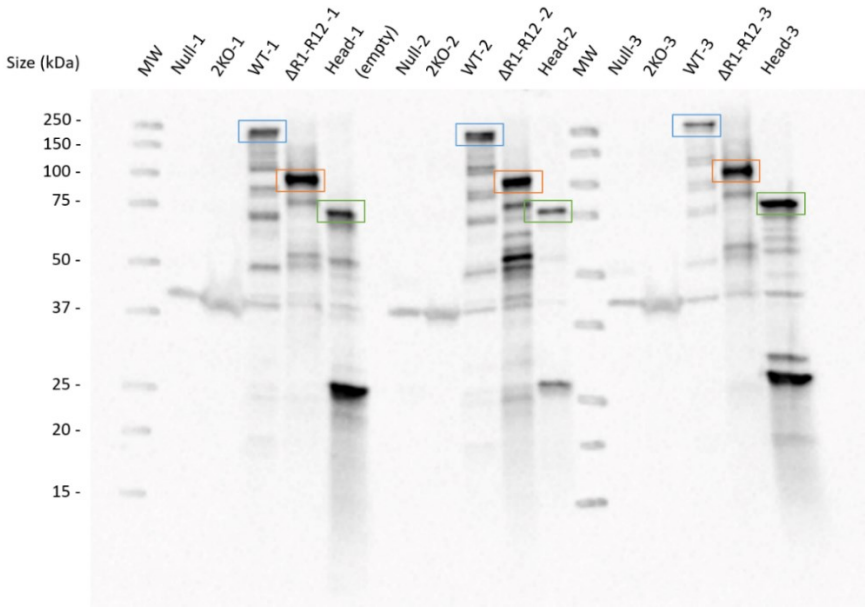

Figure 9. *Western blot image for talin, stained with Goat Anti-GFP (#AB0020-500, Sicgen) and Peroxidase labeled Anti-Goat IgG (H+L) affinity purified made in Horse (#PI-9500, Vector Laboratories). The bands corresponding to different talin variants are high-lighted.*

The intensities of the bands were measured as areas with signal, and then the intensities of the constructs were compared to actin that acted as a loading control to obtain relative intensities. The results are presented in Table 2 and Figure 10.

Table 2. *Intensities of talin expression measured from Western blot images. The relative intensities are calculated by dividing the values of talin by the values of actin.*

Sample	Area (Intensity)	Sample	Area (Intensity)	Relative intensity
WT		Actin (std)		
1	20599	1	22298	0.9
2	24508	2	12839	1.9
3	14012	3	15740	0.9
ΔR1-R12				
1	27962	1	8797	3.2
2	24847	2	20998	1.2
3	24147	3	13649	1.8
Head				
1	18958	1	7235	2.6
2	9588	2	2021	4.7
3	26419	3	22192	1.2

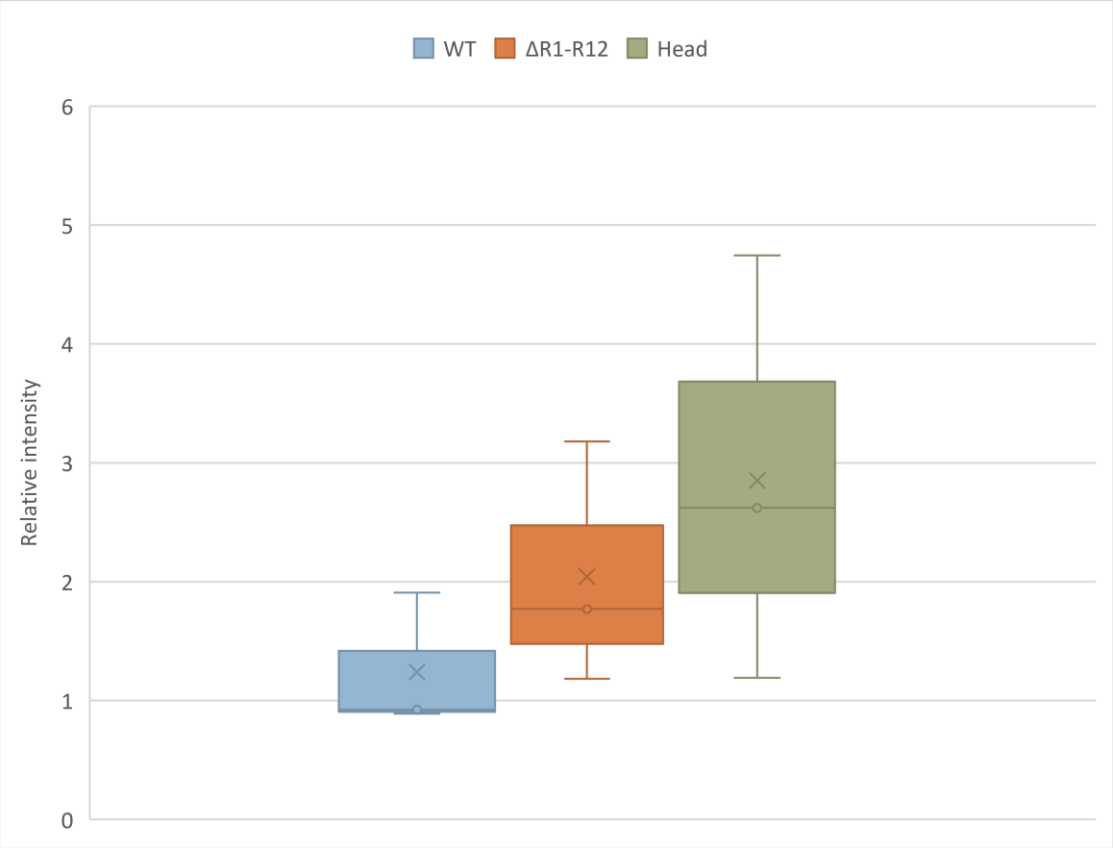

Figure 10. *Relative intensity of talin expression in graphic form.*

5.4 Confocal imaging to determine subcellular localization of talin forms

Representative confocal images obtained from the three talin constructs are presented in Figure 11. The images were taken from channels 405 nm (DAPI) and 488 nm (GFP) and merged to display both. All the focal planes acquired in imaging were combined in ImageJ by Z-projection set to maximum intensity to display the cells with sufficient clarity.

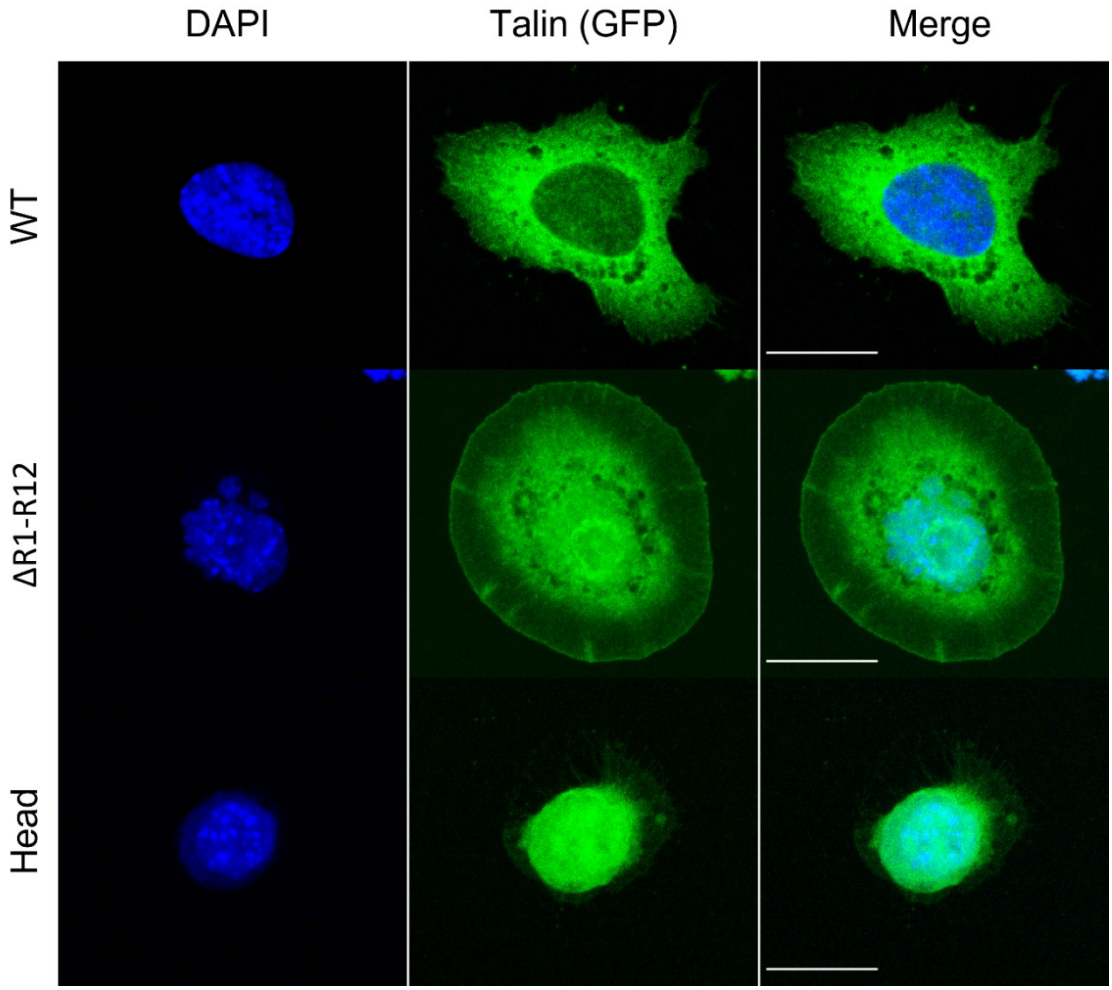

Figure 11. *Subcellular localization of the talin forms. Confocal images of cells expressing full-length WT talin, ΔR1-R12 talin and talin head are shown, taken from channels 405 nm (DAPI) and 488 nm (GFP), merged in the third column. All focal planes were combined by Z-projection set to max intensity. Scale bar is 20 µm.*

The measured raw integrated densities of GFP signal inside the nucleus were compared to the values obtained from the area of the whole cell (N = 30 for each construct) to calculate the percentage in which talin had entered the nucleus, represented by relative integrated density.

The analysis was conducted as follows in ImageJ: first the centre of the nucleus was determined on DAPI channel at the focal plane where the nucleus was at its widest (the nucleus was outlined by freehand selection tool), and then 3 other focal planes where the area of the nucleus was roughly the same were chosen around it. These 4 planes were combined by Z-projection set to average intensity on GFP channel, where the raw integrated density of the signal was first measured within the bounds of the nucleus (selection transferred from DAPI channel) and then within the estimated area of the whole cell, nucleus included. These two values were then compared.

Statistical analysis was conducted using one-way ANOVA with Bonferroni test. $P \leq 0.05$ was considered statistically significant. Statistical data involving the mean and standard deviation of the obtained values for each construct is presented in Table 3. Graph of the results is presented in Figure 12.

Table 3. *Statistical data from comparing the raw integrated densities of GFP signal inside the nucleus to the whole cell.*

Relative integrated density - nucleus vs whole cell (%)			
Sample	N	Mean	Std. Dev.
WT	30	16.63	3.09
∆R1-R12	30	20.45	3.43
Head	30	46.58	9.88

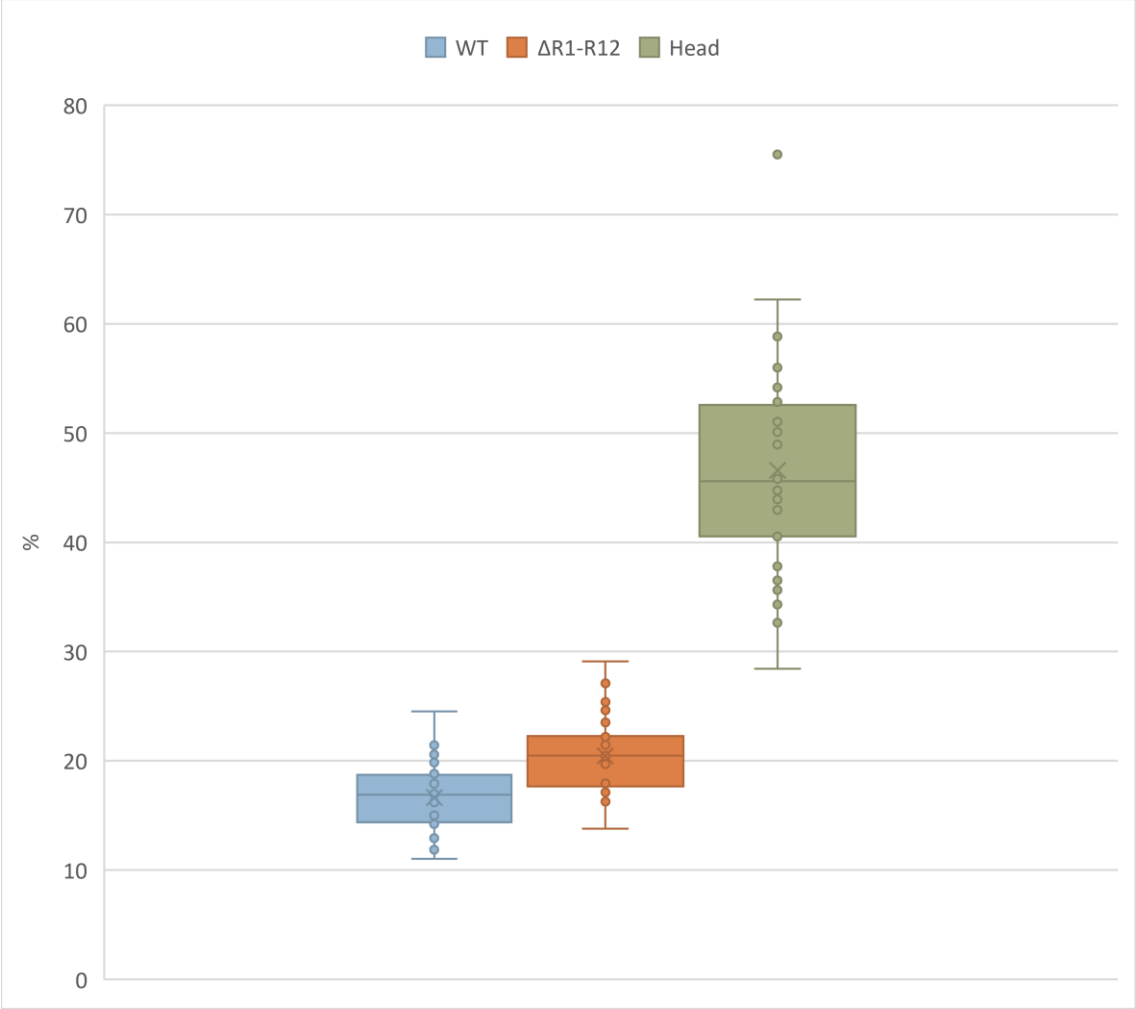

Figure 12. *Relative amount of talin in the nucleus vs the whole cell, obtained from comparing the raw integrated densities of GFP signal inside the nucleus to the whole cell.*

5.5 Prediction of subcellular localization

We used WoLF PSORT program to get additional information about the subcellular localization of the talin forms. The program compares the amino acid sequence of the query to datasets of proteins with known localization sites to obtain a value for *k*-nearest neighbour classifier, indicating sequence similarity (Horton et al., 2007). This value can be used to predict the likelihood of localization site. The results are shown in Table 4.

Table 4. *Prediction of the localization sites of the talin forms with WoLF PSORT program. Values are displayed as k-nearest neighbour classifiers (higher = more likely).*

	Predicted localization site		
Sample	Cytosol	Cytosol/nucleus	Nucleus
WT	12.0	13.5	13.0
ΔR1-R12	17.5	13.5	8.5
Head	21.0	12.7	2.0

6. DISCUSSION

The main focus of this thesis was on the role of talin as a part of the nucleo-adhesome that includes several adhesion proteins localizing to the nucleus (Byron et al., 2022). In a recent study by Da Silva et al. (2022) it was shown that talin enters the nucleus, interacts with chromatin and alters the gene expression profile of the cell. Specifically, in the absence of talin-1, 318 genes are upregulated while 419 of them are downregulated. In our study, we evaluated the effect of replacing genomic Tln1 with plasmids of following constructs: full-length wild-type Tln1, Tln1 ∆R1-R12 (head + R13 + DD) and Tln1 ∆R1-R13 (talin head). We witnessed this effect in the gene expression profile of the cells determined by quantifying the isolated mRNA, as well as the subcellular localization of the talin forms within the cells, observed by confocal imaging.

At first, the protein quantification was solely done to evaluate the functionality of the plasmids regarding whether the inserted genes were actually translated into proteins. The Western blot confirmed that the expected proteins were produced successfully, as their bands appeared at positions close to their respective size markers (WT = 270 kDa, ∆R1-R12 = 109 kDa and head = 79 kDa). However, the expression levels can't be reliably evaluated from the results because the bigger proteins don't transfer as well from gel to membrane as smaller ones. That's why the lower intensity of WT talin in Figure 9 may be a result of poor transfer rather than weak protein expression. As these results were supposed to be qualitative to begin with, cell numbers in each sample weren't standardized. The inconsistencies can easily be seen in the Figure 8 as even the amount of actin in 2KO cells is much higher compared to other cells, reflecting the amount of total protein in the sample. However, the obtained results are sufficient proof of a functional system.

The results of the differential gene expression analysis (Figure 7) were partially as expected, but also had some surprising elements. There were naturally differences between talin DKO cells and other cells, greater number of genes clearly being downregulated in DKO cells compared to talin-2KO cells. This is in line with previous research, as absence of talin-1 seems to cause more downregulation than upregulation (Da Silva et al., 2022), even though the numbers in our study are higher (N_{up}(DKO vs 2KO) = 3404/N_{down} = 3786). However, we used a different cell line. It's also notable that there isn't as much difference between DKO cells and cells expressing talin head as in other comparisons with DKO (N_{all}(DKO vs head) = 3394, while N_{all}(DKO vs X ≠ head) > 5000). The finding is somewhat surprising given the fact that talin head showed strong localization into cell nucleus (Figure 12). This might indicate that although talin head appears

important for nuclear localization, mere head domain doesn't have significant influence on gene expression. There are also considerably little differences between the constructs (N_{all}(construct X vs construct Y) < 3000, while N_{all}(control X vs construct X) > 3000), although full-length WT talin seems to cause more gene expression upregulation within this category (N_{up}(WT vs ∆R1-R12) = 685/N_{down} = 416, N_{up}(WT vs head) = 1435/N_{down} = 1198).

The differences between talin-2KO cells and the cells with transfected WT talin (N_{all}(2KO vs WT) = 9073 and N_{all}(DKO vs 2KO) = 7190 compared to N_{all}(DKO vs WT) = 6211) are interesting: this may indicate that genomic and ectopic talin are treated differently by the cell, with genomic talin-1 causing a bit more upregulation (N_{up}(2KO vs WT) = 4545/N_{down} = 4528). This difference between genomic and ectopic talin can also be seen with the other constructs (N_{all}(2KO vs construct X) > 8000). The limitation of this study was that it only analysed overall gene expression – in the future the expression levels of individual genes should be studied.

The cell morphology in the confocal images (Figure 11) was as expected from previous research (Rahikainen et al., 2019). Full-length WT talin causes the presentation of a polarized shape, where talin localizes to the cytosol. Also, lamellipodium is clearly formed in these cells compared to the other specimens, indicating that talin also localizes to the plasma membrane, where it participates in the formation of focal adhesions. There's visibly less green fluorescence inside the nucleus in cells expressing full-length WT talin as compared to other talin forms. The only GFP aggregates are at the nucleoli that correspond to the darker areas of the DAPI staining in Figure 11. This is an established phenomenon (Da Silva et al., 2022). ∆R1-R12 talin leads to an isotropic, but spread cell shape, where talin is mostly located in the cytosol and less at the plasma membrane. Expression of mere talin head yields a globular cell shape with very little spreading, where talin is predominantly located in the cytosol and possibly also in the nucleus.

The image analysis was in line with visual cues, as there indeed was talin inside the nuclei of all the transfected cells, the amount varying between the constructs. It was already established in previous research that talin-1 enters the nucleus, concentrating in the nucleoli (Da Silva et al., 2022). In our study, around 17% of full-length WT talin and 20% of ∆R1-R12 talin enter the nucleus. No statistically significant difference exists between these two ($P = 0.11$), so the amount can be considered the same. On the other hand, around 47% of talin head resides inside the nucleus, with clear statistically significant differences compared to other samples ($P < 0.001$). These results indicate that full-length WT talin and ∆R1-R12 talin are similar in their lower efficiency of nuclear localization compared to talin head, which could be linked to their better capability to accumulate

into integrin adhesion structures at the plasma membrane, leaving less of these molecules to localize to the nucleus. Moreover, differential gene expression analysis also revealed the most similar profiles for WT and ∆R1-R12 talin in relation to other comparisons (N_{all}(WT vs ∆R1-R12) = 1101)(Figure 7), even though this difference is still remarkable in of itself.

Meanwhile, talin head enters the nucleus in great amount, even though its gene expression profile is closer to the one of talin DKO cells, which is interesting. One reason for this may be the small size of the talin head domain (79 kDa) which might make passive diffusion through nuclear pores possible, as up to 60 kDa size molecules pass through them rather freely, rates gradually decreasing beyond that threshold (Timney et al., 2016). If this is not the sole reason, there's an indication that the FERM domain contains the nuclear localization signal. In previous research it has been hypothesized that proteins with FERM domain act as information mediators between the plasma membrane and the nucleus – one confirmed example of this is FAK that acts as a transcription regulator (Da Silva et al., 2022). With FAK, there are also indications that the NLS is indeed within its FERM domain (Brami-Cherrier et al., 2014).

It is possible that talin behaves similarly to FAK in regards of nuclear localization, but this has yet to be studied along with the exact location of the NLS. In the prediction we made with WoLF PSORT (Table 4), all the talin forms got at least the second-most similarity to proteins that shuttle between the cytosol and the nucleus (WT and ∆R1-R12 = 13.5 and head = 12.7), which backs the hypothesis of the NLS being in the head domain. In this case, the FERM domain of the isolated talin head might be enough to trigger nuclear translocation, even though the molecule itself isn't a functional regulator of gene expression. Interestingly, ∆R1-R12 talin affects gene expression similarly to both talin head and full-length WT talin (N_{all}(WT vs ∆R1-R12) = 1101 and (N_{all}(head vs ∆R1-R12) = 1140), while there is a greater difference between WT and talin head (N_{all}(WT vs head) = 2633) (Figure 7). This might mean that talin head and ∆R1-R12 talin share some functionality, but mere head domain is still highly dysfunctional at gene expression regulation compared to full-length WT talin.

It should also be noted that the RNA sequencing we ordered only took mRNA into account while there are indications that talin localizes to the nucleoli and interacts with rRNA precursors, thus possibly playing a part in rRNA maturation (Da Silva et al., 2022). In the future rRNA quantification may be a relevant next step in understanding the function of talin inside the nucleus.

7. CONCLUSIONS

Talin is known best as a member of the integrin adhesome, a group of proteins associated with integrin adhesion complexes. It acts as an adaptor between integrin and the actin cytoskeleton of the cell along with several other proteins (Klapholz & Brown, 2017). Specifically, talin can be considered the core of these structures that enable the formation of focal adhesions (Kanchanawong et al., 2010). These qualities are related to the mechanosensitive nature of the protein, presented in the unique way talin can conform to tension by unwinding its rod domain and unveiling hidden binding sites (Gough & Goult, 2018).

In this thesis we focused on the role of talin as a part of the nucleo-adhesome that involves adhesion proteins that localize to the nucleus for different – often pathological – reasons (Byron et al., 2022). The study that acted as a starting point for my thesis showed that talin enters the nucleus, interacts with chromatin and alters the gene expression profile of the cell (Da Silva et al., 2022). In our study, we wished to find out whether similar patterns could be observed with truncated talin forms lacking an increasing number of rod subdomains.

Expressing the truncated talin forms in mouse kidney fibroblasts was successful, and the cells attained similar phenotypes to previously documented ones (Rahikainen et al., 2019). The differential gene expression levels of the cells were partially as expected: negative control had a more downregulated profile while the positive control had a more upregulated one. What was interesting, however, was the finding that the cells treated genomic and ectopic talin in distinct ways. The profiles of each construct had little difference between each other, but full-length WT talin had a more upregulating effect overall.

Regarding the nuclear localization of each talin form, around 20% of full-length WT talin and ∆R1-R12 talin entered the nucleus, while the corresponding value for talin head was around 47%. The lower nuclear localization efficiency may correlate with better localization to IACs, while the higher value for talin head may be explained by its small size or by the likely fact that there is a nuclear localization signal within the FERM domain (Byron et al., 2022). Based on confocal imaging, there are also indications that talin localizes specifically to the nucleoli, which is an established phenomenon (Da Silva et al., 2022).

Possible future tasks involve the quantification of mRNA from individual genes as well as rRNA from nucleoli when different talin forms are introduced to the cells. The location of NLS within the talin molecule should also be confirmed.

REFERENCES

Azizi, L., Cowell, A. R., Mykuliak, V. V, Goult, B. T., Turkki, P., & Hytönen, V. P. (2021). Cancer associated talin point mutations disorganise cell adhesion and migration. *Scientific Reports*, *11*(1), 347. https://doi.org/10.1038/s41598-020-77911-4

Azizi, L., Varela, L., Turkki, P., Mykuliak, V. V, Korpela, S., Ihalainen, T. O., Church, J., Hytönen, V. P., & Goult, B. T. (2022). Talin variant P229S compromises integrin activation and associates with multifaceted clinical symptoms. *Human Molecular Genetics*, ddac163. https://doi.org/10.1093/hmg/ddac163

Bachmann, M., Su, B., Rahikainen, R., Hytönen, V. P., Wu, J., & Wehrle-Haller, B. (2023). ConFERMing the role of talin in integrin activation and mechanosignaling. *Journal of Cell Science*, *136*(8), jcs260576. https://doi.org/10.1242/jcs.260576

Brami-Cherrier, K., Gervasi, N., Arsenieva, D., Walkiewicz, K., Boutterin, M.-C., Ortega, A., Leonard, P. G., Seantier, B., Gasmi, L., Bouceba, T., Kadaré, G., Girault, J.-A., & Arold, S. T. (2014). FAK dimerization controls its kinase-dependent functions at focal adhesions. *The EMBO Journal*, *33*(4), 356–370. https://doi.org/10.1002/embj.201386399

Byron, A., & Frame, M. C. (2016). Adhesion protein networks reveal functions proximal and distal to cell-matrix contacts. *Current Opinion in Cell Biology*, *39*, 93–100. https://doi.org/10.1016/j.ceb.2016.02.013

Byron, A., Griffith, B. G. C., Herrero, A., Loftus, A. E. P., Koeleman, E. S., Kogerman, L., Dawson, J. C., McGivern, N., Culley, J., Grimes, G. R., Serrels, B., von Kriegsheim, A., Brunton, V. G., & Frame, M. C. (2022). Characterisation of a nucleo-adhesome. *Nature Communications*, *13*(1), 3053. https://doi.org/10.1038/s41467-022-30556-5

Da Silva, A. J., Hästbacka, H. S. E., Puustinen, M. C., Pessa, J. C., Goult, B. T., Jacquemet, G., Henriksson, E., & Sistonen, L. (2022). A subpopulation of Talin 1 resides in the nucleus and regulates gene expression. *BioRxiv*, 2022.03.15.484419. https://doi.org/10.1101/2022.03.15.484419

del Rio, A., Perez-Jimenez, R., Liu, R., Roca-Cusachs, P., Fernandez, J. M., & Sheetz, M. P. (2009). Stretching single talin rod molecules activates vinculin binding. *Science (New York, N.Y.)*, *323*(5914), 638–641. https://doi.org/10.1126/science.1162912

DeWane, G., Salvi, A. M., & DeMali, K. A. (2021). Fueling the cytoskeleton – links between cell metabolism and actin remodeling. *Journal of Cell Science*, *134*(3). https://doi.org/10.1242/jcs.248385

Elosegui-Artola, A., Trepat, X., & Roca-Cusachs, P. (2018). Control of Mechanotransduction by Molecular Clutch Dynamics. *Trends in Cell Biology*, *28*(5), 356–367. https://doi.org/10.1016/j.tcb.2018.01.008

Gough, R. E., & Goult, B. T. (2018). The tale of two talins - two isoforms to fine-tune integrin signalling. *FEBS Letters*, *592*(12), 2108–2125. https://doi.org/10.1002/1873-3468.13081

Han, S. J., Azarova, E. V, Whitewood, A. J., Bachir, A., Guttierrez, E., Groisman, A., Horwitz, A. R., Goult, B. T., Dean, K. M., & Danuser, G. (2021). Pre-complexation of talin and vinculin without tension is required for efficient nascent adhesion maturation. *ELife*, *10*, e66151. https://doi.org/10.7554/eLife.66151

Horton, P., Park, K.-J., Obayashi, T., Fujita, N., Harada, H., Adams-Collier, C. J., & Nakai, K. (2007). WoLF PSORT: protein localization predictor. *Nucleic Acids Research*, *35*(Web Server issue), W585-7. https://doi.org/10.1093/nar/gkm259

Hytönen, V. P., & Vogel, V. (2008). How force might activate talin's vinculin binding sites: SMD reveals a structural mechanism. *PLoS Computational Biology*, *4*(2), e24. https://doi.org/10.1371/journal.pcbi.0040024

Kadrmas, J. L., & Beckerle, M. C. (2004). The LIM domain: from the cytoskeleton to the nucleus. *Nature Reviews Molecular Cell Biology*, *5*(11), 920–931. https://doi.org/10.1038/nrm1499

Kanchanawong, P., Shtengel, G., Pasapera, A. M., Ramko, E. B., Davidson, M. W., Hess, H. F., & Waterman, C. M. (2010). Nanoscale architecture of integrin-based cell adhesions. *Nature*, *468*(7323), 580–584. https://doi.org/10.1038/nature09621

Klapholz, B., & Brown, N. H. (2017). Talin – the master of integrin adhesions. *Journal of Cell Science*, *130*(15), 2435–2446. https://doi.org/10.1242/jcs.190991

Kumar, A., Anderson, K. L., Swift, M. F., Hanein, D., Volkmann, N., & Schwartz, M. A. (2018). Local Tension on Talin in Focal Adhesions Correlates with F-Actin Alignment at the Nanometer Scale. *Biophysical Journal*, *115*(8), 1569–1579. https://doi.org/10.1016/j.bpj.2018.08.045

Lawson, C., Lim, S.-T., Uryu, S., Chen, X. L., Calderwood, D. A., & Schlaepfer, D. D. (2012). FAK promotes recruitment of talin to nascent adhesions to control cell motility. *The Journal of Cell Biology*, *196*(2), 223–232. https://doi.org/10.1083/jcb.201108078

Lim, S.-T., Chen, X. L., Lim, Y., Hanson, D. A., Vo, T.-T., Howerton, K., Larocque, N., Fisher, S. J., Schlaepfer, D. D., & Ilic, D. (2008). Nuclear FAK promotes cell proliferation and survival through FERM-enhanced p53 degradation. *Molecular Cell*, *29*(1), 9–22. https://doi.org/10.1016/j.molcel.2007.11.031

Manso, A. M., Okada, H., Sakamoto, F. M., Moreno, E., Monkley, S. J., Li, R., Critchley, D. R., & Ross, R. S. (2017). Loss of mouse cardiomyocyte talin-1 and talin-2 leads to β-1 integrin reduction, costameric instability, and dilated cardiomyopathy. *Proceedings of the National Academy of Sciences of the United States of America*, *114*(30), E6250–E6259. https://doi.org/10.1073/pnas.1701416114

Monkley, S. J., Zhou, X.-H., Kinston, S. J., Giblett, S. M., Hemmings, L., Priddle, H., Brown, J. E., Pritchard, C. A., Critchley, D. R., & Fässler, R. (2000). Disruption of the talin gene arrests mouse development at the gastrulation stage. *Developmental Dynamics*, *219*(4), 560–574. https://doi.org/https://doi.org/10.1002/1097-0177(2000)9999:9999<::AID-DVDY1079>3.0.CO;2-Y

Park, J. S., Burckhardt, C. J., Lazcano, R., Solis, L. M., Isogai, T., Li, L., Chen, C. S., Gao, B., Minna, J. D., Bachoo, R., DeBerardinis, R. J., & Danuser, G. (2020). Mechanical regulation of glycolysis via cytoskeleton architecture. *Nature*, *578*(7796), 621–626. https://doi.org/10.1038/s41586-020-1998-1

Rahikainen, R., Öhman, T., Turkki, P., Varjosalo, M., & Hytönen, V. P. (2019). Talin-mediated force transmission and talin rod domain unfolding independently regulate adhesion signaling. *Journal of Cell Science*, *132*(7). https://doi.org/10.1242/jcs.226514

Schulte, C., Ferraris, G. M. S., Oldani, A., Galluzzi, M., Podestà, A., Puricelli, L., de Lorenzi, V., Lenardi, C., Milani, P., & Sidenius, N. (2016). Lamellipodial tension, not integrin/ligand binding, is the crucial factor to realise integrin activation and cell migration. *European Journal of Cell Biology*, *95*(1), 1–14. https://doi.org/10.1016/j.ejcb.2015.10.002

Schwartz, M. A. (2010). Integrins and extracellular matrix in mechanotransduction. *Cold Spring Harbor Perspectives in Biology*, *2*(12), a005066. https://doi.org/10.1101/cshperspect.a005066

Smith, M. A., Hoffman, L. M., & Beckerle, M. C. (2014). LIM proteins in actin cytoskeleton mechanoresponse. *Trends in Cell Biology*, *24*(10), 575–583. https://doi.org/10.1016/j.tcb.2014.04.009

Sun, Z., Guo, S. S., & Fässler, R. (2016). Integrin-mediated mechanotransduction. *Journal of Cell Biology*, *215*(4), 445–456. https://doi.org/10.1083/jcb.201609037

Theodosiou, M., Widmaier, M., Böttcher, R. T., Rognoni, E., Veelders, M., Bharadwaj, M., Lambacher, A., Austen, K., Müller, D. J., Zent, R., & Fässler, R. (2016). Kindlin-2 cooperates with talin to activate integrins and induces cell spreading by directly binding paxillin. *ELife*, *5*, e10130. https://doi.org/10.7554/eLife.10130

Timney, B. L., Raveh, B., Mironska, R., Trivedi, J. M., Kim, S. J., Russel, D., Wente, S. R., Sali, A., & Rout, M. P. (2016). Simple rules for passive diffusion through the nuclear pore complex. *The Journal of Cell Biology*, *215*(1), 57–76. https://doi.org/10.1083/jcb.201601004

Turley, T. N., Theis, J. L., Sundsbak, R. S., Evans, J. M., O'Byrne, M. M., Gulati, R., Tweet, M. S., Hayes, S. N., & Olson, T. M. (2019). Rare Missense Variants in TLN1 Are Associated With Familial and Sporadic Spontaneous Coronary Artery Dissection. *Circulation. Genomic and Precision Medicine*, *12*(4), e002437. https://doi.org/10.1161/CIRCGEN.118.002437

Vicente-Manzanares, M., & Horwitz, A. R. (2011). Adhesion dynamics at a glance. *Journal of Cell Science*, *124*(23), 3923–3927. https://doi.org/10.1242/jcs.095653